

# Solvent-Adoptable Polymer Ni/NiCo Alloy Nanochains: Highly Active and Versatile Catalysts for Various Organic Reactions in both Aqueous and Nonaqueous Media

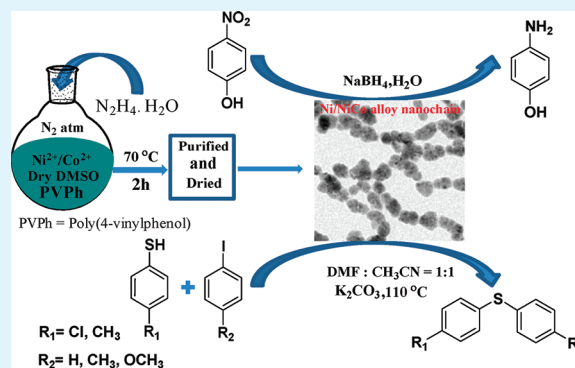
Manoj Raula, Md. Harunar Rashid, Sima Lai, Mouni Roy, and Tarun K. Mandal\*

Polymer Science Unit, Indian Association for the Cultivation of Science, Jadavpur, Kolkata 700 032, India

## Supporting Information

**ABSTRACT:** The synthesis of solvent-adoptable monometallic Ni and NiCo alloy nanochains by a one-pot solution phase reduction method in the presence of poly(4-vinylphenol) (PVPh) is demonstrated. The elemental compositions of the as-prepared alloys are determined by inductively coupled plasma optical emission spectroscopy (ICP-OES) and energy-dispersive X-ray spectroscopy (EDS), which are matching well with the target compositions. The morphology analysis by TEM and FESEM confirms that the nanochains are made up of organized spherical monometallic Ni or bimetallic NiCo alloy nanoparticles (NPs). However, there is no nanochain formation when the alloy is prepared without the polymer PVPh. A possible mechanism for the formation of such NiCo alloy nanochains is discussed. The X-ray diffraction and selected area electron diffraction patterns reveal that the Ni/NiCo alloys are polycrystalline with fcc structure. The obtained Ni or NiCo alloy nanostructures are ferromagnetic with very high coercivity. The polymer Ni/NiCo alloy nanochains are dispersible in both water and organic media that makes them versatile enough to use as catalysts in the reactions carried out in both types of media. The catalytic activities of these Ni/NiCo alloy nanochains are extremely high in the borohydride reduction of *p*-nitrophenol in water. In organic solvents, these nanochains can act as efficient catalysts, under ligand-free condition, for the C–S cross-coupling reactions of various aryl iodides and aryl thiols for obtaining the corresponding cross-coupled products in good to excellent yield up to 96%. The NiCo nanochain also successfully catalyzes the C–O cross-coupling reaction in organic medium. A possible mechanism for NiCo alloy nanochain-catalyzed cross-coupling reaction is proposed.

**KEYWORDS:** polymer, NiCo, alloy, nanochains, catalysts, organic reactions, solvent adoptable



## INTRODUCTION

Nowadays, transition metals and their bimetallic alloy nanostructures have become increasingly interesting to scientists and engineers because of their wide range of physicochemical properties for applications in diverse areas such as optical,<sup>1</sup> data storage,<sup>2</sup> magnetic recording media,<sup>3</sup> contrast agent in magnetic resonance imaging (MRI),<sup>4</sup> cancer therapy,<sup>5</sup> and catalysis.<sup>6,7</sup> But, very recently, especially bimetallic alloy nanoparticles (NPs) are of great interest in diverse areas such as catalysis<sup>7</sup> and biomedical,<sup>8</sup> not only because of size effects but also as a result of the combination of different metals in terms of large diversity in the composition, structures and various properties.<sup>9</sup> Some system generates core–shell alloy structure, where overlayer is usually strained, and thus can present peculiar catalytic properties.<sup>10</sup> Consequently, several different approaches have been developed to synthesize nanostructured bimetallic alloys, such as, FeNi,<sup>11</sup> NiPt,<sup>12</sup> NiPd,<sup>13</sup> FePt,<sup>14</sup> PtCo,<sup>15</sup> FeCo,<sup>14</sup> NiCo,<sup>16–22</sup> and CuNi<sup>23</sup> of various shapes and sizes. For example, homogeneous NiCo alloy nanowire were prepared by gas–solid–solid phase method at very high temperature (~ 900 °C).<sup>24</sup> Various

solution-based techniques such as, chemical reduction by strong reducing agents (hydrazine or NaBH<sub>4</sub>),<sup>19,25</sup> emulsion/micro-emulsion synthesis,<sup>26</sup> polyol methods,<sup>27</sup> microwave method,<sup>20</sup> and hydrothermal reactions<sup>16,21,22,28</sup> were utilized for the preparation of spherical,<sup>21</sup> flowerlike,<sup>19</sup> chainlike,<sup>19,25</sup> and braceletlike<sup>28</sup> NiCo alloy nanostructures. However, the reported chainlike NiCo alloy nanostructures are constituted of spherical NPs of sizes bigger than 50 nm with high polydispersity.<sup>22,25</sup> Also, the length of the obtained alloy chain is not so long. From the application point of view, it is important that chainlike (one-dimensional) structural materials should be made up of particles with very low diameter and uniform size, which are likely to play a critical role in the improvement of the efficiencies of various devices. Therefore, our aim is to synthesize nanochains consisting of nearly monodisperse NiCo alloy NPs of smaller sizes.

These nanoalloys are susceptible to the aerial oxidation, and thus, to protect them, various capping/protecting agents such

Received: November 7, 2011

Accepted: January 5, 2012

Published: January 5, 2012

as long chain acids,<sup>29</sup> amines,<sup>20</sup> phosphine oxides,<sup>30</sup> polymers,<sup>28,31,32</sup> and surfactants<sup>26,29</sup> are often used during their synthesis. These protecting agents sometime can also control the shape of the alloy NPs.<sup>33</sup> In this context, polymers become increasingly popular choice to the researchers. But, to date, only very few polymers such as poly(vinylpyrrolidone),<sup>16,28</sup> poly(ethylene glycol),<sup>34</sup> and pluronic triblock copolymer<sup>35</sup> have been used to synthesize transition metal alloy NPs. Very recently, our group has synthesized NiCo alloy nanochains using poly(methyl vinyl ether).<sup>25</sup> But, to date, no one has used poly(4-vinylphenol) (PVPh) to synthesize NiCo alloy nanostructures. PVPh is an important polymer, soluble in nonaqueous solvents as well as in water under alkaline condition, and behaves like a polyelectrolyte. Earlier, we used PVPh for generation of spherical gold NPs.<sup>36</sup>

It is known that transition metals including many expensive metals such as Pd, Au, and Pt and their alloy NPs are promising candidates as catalysts for various organic and inorganic reactions.<sup>37–41</sup> For example, the borohydride reduction of *p*-nitrophenol in water is an important organic reaction that has been extensively studied to explore the catalytic activities of numerous transition metal and their alloy NPs including NiCo alloy NPs.<sup>13,25,40,42–48</sup> However, we are the first to use NiCo alloy nanostructures as successful catalysts for this reaction.<sup>25</sup> Besides the above reactions, the C–S, C–O, and C–N bond formation via cross-coupling reaction is also important organic reactions for preparing several compounds that are important in pharmaceutical,<sup>49,50</sup> biological, and material chemistry.<sup>37,51,52</sup> However, most of these cross-coupling reactions have been carried out in homogeneous organic phase using transition metal complexes comprising of various ligands. But, the uses of metal and their alloy nanostructures with high surface area as nanocatalysts are advantageous in terms of ease of product isolation, recovery and reusability of the catalysts. Consequently, different MNPs (mostly Cu NPs) were used as catalysts for these bond formation reactions.<sup>39,53,54</sup> But, to the best of our knowledge, there exists no report on the use of the bimetallic NiCo alloy NPs as catalysts for these cross-coupling reactions, beside our recent preliminary work on the catalysis of C–S bond formation.<sup>25</sup>

In this manuscript, we report a low-temperature solvothermal synthesis of long chainlike monometallic Ni and bimetallic NiCo alloy nanostructures using hydrazine as reducing agent and poly(4-vinylphenol) (PVPh) as a capping-cum-shape directing agent in DMSO. It is shown that no chain-like NiCo alloy NPs is generated without PVPh. The obtained NiCo alloy nanochain shows very high catalytic activity (probably highest) for the borohydride reduction of *p*-nitrophenol in water. Previously, we have reported preliminary results demonstrating that the NiCo alloy NPs can be used as catalyst for the C–S cross-coupling reaction only between 4-chlorothiophenol and iodobenzene.<sup>25</sup> But, the yield of the reaction was very poor (~30%). Here, we report the detailed investigation of the C–S cross-coupling reactions involving different substituted thiophenols and aryl iodides using long chainlike NiCo alloy nanostructures in mixture of organic solvents. In most of the cases, we obtained good to excellent yields. It is also shown that the obtained long NiCo alloy nanochains can act as catalyst for the C–O cross-coupling reactions. Finally, it is shown that the obtained NiCo nanoalloys can be easily separated from the reaction mixture using a bar magnet and can be reused in the *p*-nitrophenol reduction reaction up to seven cycles.

## EXPERIMENTAL SECTION

**Materials.** Nickel(II) acetylacetonate, [Ni(acac)<sub>2</sub>] (Aldrich), cobalt(II) acetylacetonate, [Co(acac)<sub>2</sub>] (Aldrich), poly(4-vinylphenol) (PVPh) (*M<sub>w</sub>* ≈ 11 000) (Aldrich) and hydrazine (N<sub>2</sub>H<sub>4</sub>) 80% aqueous solution (Loba Chemicals, India) were used as received. Dimethyl sulphoxide (DMSO) (kept over CaCl<sub>2</sub> for 2 days and then stirred about 12 h using CaH<sub>2</sub>, finally distilled under vacuum) (Merck India), ethyl alcohol (Bengal Chemicals, India), dimethylformamide (DMF) (Merck) (kept over CaCl<sub>2</sub> for 2 days and then stirred about 12 h using CaH<sub>2</sub>, finally distilled under vacuum), and acetonitrile (Merck) were used after distillation. Nitric acid (Merck), *p*-nitrophenol (4NP) (Merck), and sodium borohydride (NaBH<sub>4</sub>) (Spectrochem, India) were used as received. All aryl iodides, thiophenols, and 3,5-dimethyl phenol were obtained from Aldrich and used without further purification. Cesium carbonate (Cs<sub>2</sub>CO<sub>3</sub>) (Spectrochem, India) and potassium carbonate (K<sub>2</sub>CO<sub>3</sub>) (Merck, India) were used as received in inert atmosphere. Triple distilled water was used in the catalysis reaction.

**Synthesis of Polymer Ni/NiCo Alloy Nanochains.** NiCo alloy nanostructures of varying compositions were prepared by the reduction of an appropriate mixture of the Ni(acac)<sub>2</sub> and Co(acac)<sub>2</sub> salts using hydrazine in DMSO and in the presence of poly(4-vinylphenol) (PVPh). In a typical synthesis, 40.0 mL of PVPh solution in DMSO (0.2 wt %) was taken in a round-bottom flask under Ar-atmosphere with constant magnetic stirring. To this stirring solution, 0.0642 g of Co(acac)<sub>2</sub> (0.005 mol) was added. After complete dissolution of Co(acac)<sub>2</sub>, 0.0642 g of Ni(acac)<sub>2</sub> (0.005 mol) was then added and the reaction mixture was homogenized for 2 h under an Ar atmosphere. Nine milliliters of ethanolic solution of N<sub>2</sub>H<sub>4</sub> (8M) was injected at a time, followed by the addition of 1 mL of ethanolic NaOH solution (0.02 M) and the reaction mixture was heated at 70 °C for 2 h. After cooling to room temperature, 100 mL of mixture of water and ethyl alcohol (1:2) was added and the alloy sample was isolated from the suspension by using a bar magnet. This purification process was repeated several times to remove the excess reactants. Finally, the isolated nanoalloy samples were dried in vacuum at 60 °C. This polymer adsorbed alloy sample is designated as “PVPh-Ni<sub>1</sub>Co<sub>1</sub>”, where (1:1) is the initial molar feeding ratio for Co to Ni precursors. NiCo alloy nanostructures of other compositions were also prepared by varying the initial molar feeding ratio of metal precursors by the similar procedure (Table 1). Monometallic Ni nanochains were also prepared using similar procedure.

**Catalysis by Ni/NiCo Alloy Nanochains. Catalysis of Borohydride Reduction of *p*-Nitrophenol (4NP) in Water.** In a typical reaction, 0.1 mL of aqueous NaBH<sub>4</sub> solution (0.3 M) was added to a stirring reaction mixture of 2.8 mL water, 0.1 mL of aqueous 4NP solution (0.003 M) and 0.001 g of purified/dried solid NiCo alloy nanocatalyst at 25 °C. The time-dependent UV–vis absorption spectra of the reaction mixture were then recorded using a spectrophotometer. The progress of the reaction was monitored by monitoring the disappearance of the peak at λ<sub>max</sub> = 400 nm corresponds to the nitrophenolate ion due to its conversion to *p*-aminophenolate ion with the time. The catalytic activities of other NiCo nanoalloys of different compositions and neat Ni nanostructures toward this reaction were also measured using similar recipe as used for the above-mentioned reaction set. We also conducted this reaction at different temperatures (25, 35, 45, and 55 °C) using PVPh-Ni<sub>3</sub>Co<sub>1</sub> (Table 1) as the representative catalyst to measure its activation energy.

**Catalysis of the C–S Cross-Coupling Reactions in (1:1) Mixture of Acetonitrile/DMF.** The activities of as-synthesized neat Ni or NiCo alloy nanocatalysts toward a particular C–S coupling reaction were tested in organic medium. For this, typically, 224 μL of iodobenzene (2 mmol) and 288 mg of *p*-chlorothiophenol (2 mmol) were first taken in reaction vessel. Four milliliters of acetonitrile and DMF mixture (1:1) was then added to this vessel and the mixture was purged with Ar gas for a while. Then, 1.38 g of K<sub>2</sub>CO<sub>3</sub> (10 mmol) and 12 mg of either neat Ni or any NiCo alloy nanocatalysts samples were added to the reaction mixture. The mixture was then heated at 110 °C in an Ar atmosphere. After 15 h, the reaction mixture was

**Table 1. Reaction Recipe for the Synthesis of Ni/NiCo Alloy Nanostructures with and without PVPh and Their Characterizations<sup>a</sup>**

sample name	PVPh (wt %)	[Ni <sup>2+</sup> ] (M)	[Co <sup>2+</sup> ] (M)	target atomic ratio (Ni:Co)	composition (Ni:Co) <sup>b</sup> (w/w)	composition (Ni:Co) <sup>c</sup> (w/w)	yield (%)	D <sub>TEM</sub> <sup>d</sup> (nm)
PVPh-Ni	0.2	0.01		1:0			100	20 ± 2
PVPh-Ni <sub>3</sub> Co <sub>1</sub>	0.2	0.0075	0.0025	3:1	74:26	77:23	100	25 ± 4
PVPh-Ni <sub>2</sub> Co <sub>1</sub>	0.2	0.0066	0.0033	2:1	64:36	68:32	100	40 ± 5
PVPh-Ni <sub>1</sub> Co <sub>1</sub>	0.2	0.005	0.005	1:1	48:52	49:51	100	62 ± 8
PVPh-Ni <sub>1</sub> Co <sub>2</sub>	0.2	0.0033	0.0066	1:2	33:67	31:69	90	78 ± 10
Ni <sub>3</sub> Co <sub>1</sub>		0.0075	0.0025	3:1	76:24	76:24	100	<sup>e</sup>
Ni <sub>1</sub> Co <sub>1</sub>		0.005	0.005	1:1	50:50	51:49	100	<sup>e</sup>

<sup>a</sup>Conditions: solvent = dry DMSO; temperature = 70°C; time = 2 h. <sup>b</sup>Calculated from ICP-OES measurement. <sup>c</sup>Calculated from EDS analysis. <sup>d</sup>Average diameter of spherical Ni/NiCo NPs of the nanochains samples measured from TEM. <sup>e</sup>Unable to measure.

cooled to room temperature and diluted with diethyl ether (~ 20 mL). The organic phase was washed with 10% NaOH solution and then with brine solution for 4–5 times and was dried over Na<sub>2</sub>SO<sub>4</sub> and evaporated to obtain the crude products. The pure product can be obtained with the column chromatography using 200 mesh silica gel column using petroleum ether as the eluent. The cross-coupling reactions of different *p*-substituted aryl iodides and thiophenols were also carried out in presence of (10 mol %) PVPh-Ni<sub>3</sub>Co<sub>1</sub> nanocatalyst using similar reaction recipes and conditions as described above. The pure product was characterized via NMR spectroscopy.

**Catalysis of the C–O Cross-Coupling Reaction in Dry DMF.** Typically, 1.2 mmol (0.147 g) of 3,5-dimethylphenol, 112 μL of iodobenzene (1 mmol), 0.977 g of Cs<sub>2</sub>CO<sub>3</sub> (3 mmol), and 6 mg of PVPh-Ni<sub>3</sub>Co<sub>1</sub> (10 mol %) were first taken in reaction vessel. The reaction vessel was then evacuated first and then refill with Ar gas. This process was performed three times. Four milliliters of dry DMF was then added to this vessel using a syringe and the mixture was purged with Ar gas for a while. The reaction mixture was then heated at 140 °C. After 30 h, the reaction mixture was cooled to room temperature and diluted with diethyl ether (~ 20 mL). The organic phase was washed with 10% NaOH solution and then with brine solution for 4–5 times. The organic phase was dried over Na<sub>2</sub>SO<sub>4</sub> and evaporated to obtain the crude products. The pure product can be obtained with the column chromatography using 200 mesh silica gel column using petroleum ether as the eluent. The pure product was characterized via NMR spectroscopy.

**Reusability of NiCo Alloy Nanochains in the Borohydride Reduction of 4NP.** Since the synthesized NiCo alloys can be isolated easily using a bar magnet from the reaction mixture, these alloy samples can be reused for catalysis. For this, we first performed the borohydride reduction of 4NP using 1.3 mg of a representative sample PVPh-Ni<sub>3</sub>Co<sub>1</sub>. After the reaction, the catalyst was isolated using a bar magnet and was washed thoroughly with triple distilled water and was dried. The purified/dried sample (PVPh-Ni<sub>3</sub>Co<sub>1</sub>) was then used again for the catalysis of same reaction under similar conditions. The reusability experiment of the catalyst was checked up to seven times in similar fashion.

## ■ CHARACTERIZATION

The bulk compositions of the NiCo nanoalloys were determined by analyzing the samples in an inductively coupled plasma optical emission spectrometer (ICP-OES) (Optima 2100 DV, Perkin-Elmer). The alloy samples were dissolved in nitric acid (SN) before ICP-OES measurement.

For transmission electron microscopic (TEM) analysis, the dried powder samples were first redispersed in ethyl alcohol by ultrasonication. A drop of the sample's suspension was cast onto a carbon-coated copper grid and dried and imaged at an accelerating voltage of 200 kV under a JEOL high-resolution electron microscope (model JEM 2010E). Energy-dispersive

X-ray spectrum (EDS) analysis of the alloy samples were performed using an Oxford INCA system equipped with the JEOL TEM system. For each alloy sample, EDS spectra were taken from three different positions of the sample. The weight percent of elemental Ni and Co in the alloy sample was obtained from the average of these EDS data.

The X-ray diffraction measurement of the dried powder alloy and neat Ni samples were performed on a Bruker AXS D8 diffractometer at an acceleration voltage of 40 kV with 40 mA current intensity using Cu tube ( $\lambda = 0.154$  nm) as radiation source.

For FTIR characterization, the sample pellets were first prepared by mixing the alloy samples with KBr in a 1: 100 (w/w) ratio. The spectra were then acquired using this KBr pellet on a Perkin-Elmer Spectrum 400 spectrometer.

Magnetization measurements of the neat Ni and NiCo alloy samples of varying composition were carried out in a commercial Quantum Design MPMS XL (EverCool model) in the temperature range from 2–300 K with the applied magnetic field up to  $\pm 10$  kOe.

The catalytic activities of bimetallic NiCo alloys and monometallic Ni nanostructures in the borohydride reduction of *p*-nitrophenol were studied in a 1 cm path length quartz cuvette via the spectral analysis using a Hewlett-Packard 8453 diode-array spectrophotometer.

For field emission scanning electron microscopic (FESEM) study, the dried powder samples were first redispersed in ethyl alcohol by ultrasonication. A drop of the sample's suspension was cast onto a copper tape supported on a metal stub and was sputter coated with platinum to minimize charging. The images were then recorded by placing the sample under a JEOL JSM-6700F electron microscope operated at an accelerating voltage of 5 kV.

<sup>1</sup>H and <sup>13</sup>C NMR spectra of all the organic compounds in CDCl<sub>3</sub> were acquired using a Bruker DPX 300 MHz spectrometer.

Zeta potentials of the alloy NPs in suspensions in DMF/ acetonitrile (1:1) mixture were measured using Malvern Zetasizer NANO ZS 90 (model No. 3690) using HeNe gas laser of 632.8 nm.

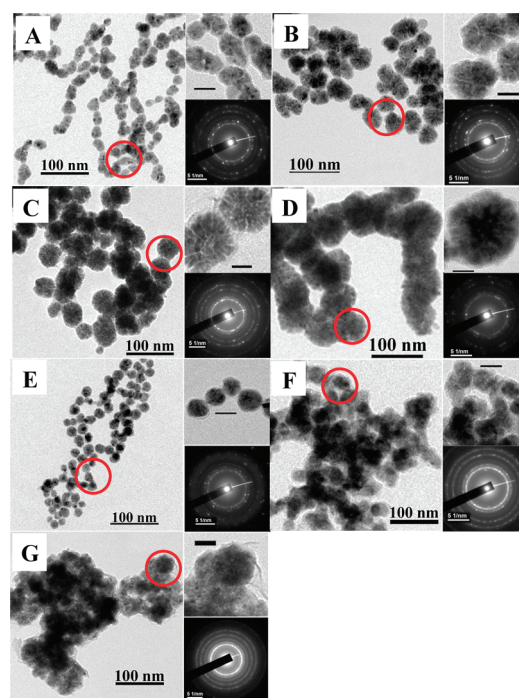
## ■ RESULTS AND DISCUSSION

**Preparation of Polymer Ni/NiCo Alloy Nanochains.** Bimetallic NiCo alloy nanostructures of four different compositions and monometallic Ni nanostructures were prepared by reduction of Ni(acac)<sub>2</sub> & Co(acac)<sub>2</sub> salts with initial molar ratios of 3:1, 2:1, 1:1, 1:2, and 1:0 using hydrazine

in the presence of poly(4-vinylphenol) (PVPPh) (Table 1). The yield is almost 100% in each case (Table 1). However, under the same experimental conditions, no cobalt (Co) NPs was formed because of the increase in reduction potential of  $\text{Co}^{2+}/\text{Co}$  system, possibly due to complex formation of  $\text{Co}^{2+}$  with DMSO (solvent).<sup>20</sup> The obtained alloy samples were dispersible in both aqueous and nonaqueous solvents (e.g., DMF, DMSO, acetonitrile, etc.) because of the adsorbed PVPPh (soluble in water and nonaqueous solvents) on their surface. The photographs of dispersions of the sample PVPPh- $\text{Ni}_3\text{Co}_1$  in different solvents such as DMSO, DMF, dioxan, acetonitrile, ethanol, water, and toluene are shown in Figure S1 in the Supporting Information. The synthesized PVPPh- $\text{Ni}_3\text{Co}_1$  alloy sample is highly dispersible in solvents like DMSO and dioxan. It shows moderately good dispersity in DMF, acetonitrile and ethanol. However, it is less dispersible in water and toluene. The adsorption of PVPPh is confirmed by FTIR spectroscopy. FTIR spectrum of the neat PVPPh exhibits bands at around 2857 and 828  $\text{cm}^{-1}$ , corresponding to the symmetric C–H stretching and the C–H out-of-plane bending of the  $-\text{CH}_2-$  group of the PVPPh polymer backbone (see Figure S2 in the Supporting Information).<sup>55</sup> The representative sample, PVPPh- $\text{Ni}_3\text{Co}_1$  also shows these two bands with a small shift toward smaller wavenumber confirming the adsorption of PVPPh at the surface of the alloy nanochains (Figure S2 in the Supporting Information). Note that the spectrum of neat  $\text{Ni}(\text{acac})_2$  does not exhibit such IR bands (Figure S2 in the Supporting Information). Control alloy samples were also prepared without PVPPh using initial molar ratio of  $\text{Ni}(\text{acac})_2:\text{Co}(\text{acac})_2 = 3:1$  and 1:1 (Table 1). The obtained alloy and neat Ni samples showed the formation of long chainlike structures, whereas the control samples did not show any such structures. The details of these morphologies will be discussed later in this section.

The weight ratios of Ni/Co in the samples PVPPh- $\text{Ni}_3\text{Co}_1$ , PVPPh- $\text{Ni}_2\text{Co}_1$ , PVPPh- $\text{Ni}_1\text{Co}_1$ , and PVPPh- $\text{Ni}_1\text{Co}_2$ , as measured from ICP-OES experiment, were found to be 74:26, 64:36, 48:52 and 33:67, respectively (Table 1). Thus, the calculated atomic ratios of Ni/Co in these samples are approximately 3:1, 2:1, 1:1, and 1:2 (atomic weights of Ni and Co are 58.7 and 58.9), respectively, which are in good agreement with the respective target atomic ratio of the alloy samples (Table 1).<sup>56</sup> The weight ratio of Ni/Co in the NiCo samples (prepared without PVPPh) also matched very well with the target atomic ratios of Ni/Co = 3 and 1 (Table 1).

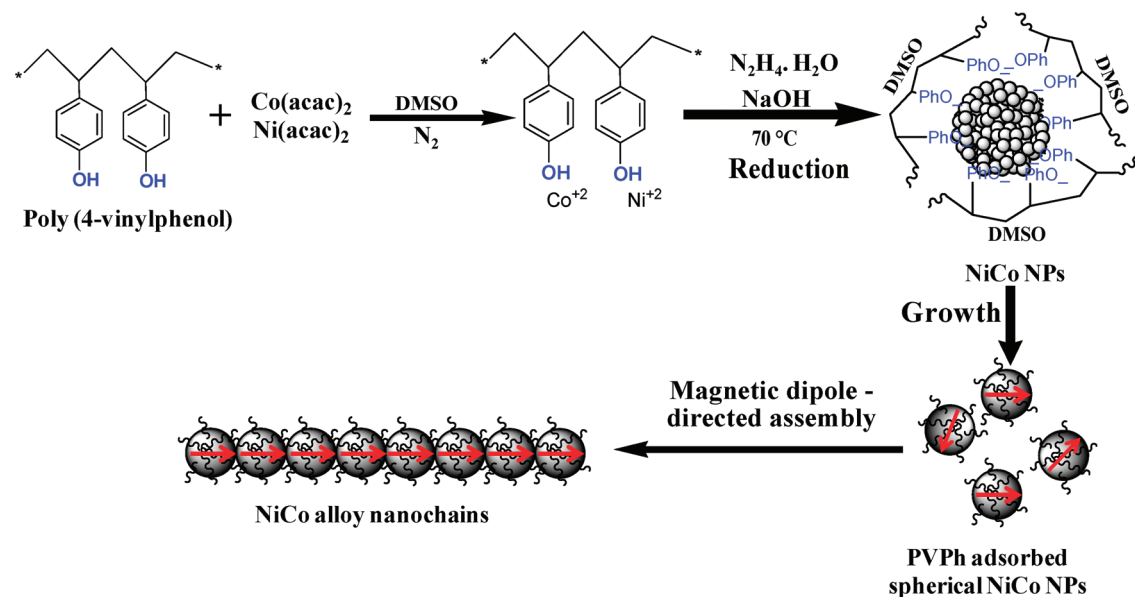
The TEM images of the as-prepared polymer NiCo alloy samples show the formation of nice long chain-like nanostructures (Figure 1 and Figure S3 in the Supporting Information). The length of the nanochains varies from 2 to 5  $\mu\text{m}$  as measured for the samples PVPPh- $\text{Ni}_3\text{Co}_1$  (Figure 1A), PVPPh- $\text{Ni}_2\text{Co}_1$  (Figure 1B), and PVPPh- $\text{Ni}_1\text{Co}_2$  (Figure 1D), which is much higher than that reported previously for alloy nanochains prepared with poly(vinyl methyl ether) (PVME).<sup>25</sup> It should be noted that the length of chain sometime even more than 5  $\mu\text{m}$  (Figure S3 in the Supporting Information). Upon closer look on a portion (highlighted in red), we noticed that these alloy chains are formed by fusion of spherical alloy NPs (upper right inserts of Figure 1A–D). As measured from these images (Figure 1A–D), the average diameters of the constituents spherical NPs of samples, PVPPh- $\text{Ni}_3\text{Co}_1$ , PVPPh- $\text{Ni}_2\text{Co}_1$ , PVPPh- $\text{Ni}_1\text{Co}_1$ , and PVPPh- $\text{Ni}_1\text{Co}_2$  are  $25 \pm 4$ ,  $40 \pm 5$ ,  $62 \pm 8$ , and  $78 \pm 10$  nm, respectively (Table 1). The TEM image of the as-prepared PVPPh-Ni sample also show similar chainlike structures that are formed by the spherical NPs of



**Figure 1.** TEM images of different polymer magnetic Ni/NiCo alloy samples (Table 1): (A) PVPPh- $\text{Ni}_3\text{Co}_1$ ; (B) PVPPh- $\text{Ni}_2\text{Co}_1$ ; (C) PVPPh- $\text{Ni}_1\text{Co}_1$ ; (D) PVPPh- $\text{Ni}_1\text{Co}_2$ ; (E) PVPPh-Ni; (F)  $\text{Ni}_3\text{Co}_1$  and (G)  $\text{Ni}_1\text{Co}_1$  prepared with/without PVPPh. The top and bottom insets in each panel, respectively, showed the magnified image and selected area electron diffraction (SAED) patterns of the specified portions (red circle) of the corresponding image. A 20 nm scale bar was shown in the upper part in the inset.

average diameter  $20 \pm 2$  nm (Figure 1E). The histograms of the particles size distribution are presented in the Figure S4 in the Supporting Information. Note that as the cobalt content in the alloys increases, the average diameter of the particles increases (Table 1). Hu et al. also observed similar type of phenomenon.<sup>16</sup> However, the control  $\text{Ni}_3\text{Co}_1$  and  $\text{Ni}_1\text{Co}_1$  sample (prepared without PVPPh) did not show such regular spherical and chain-like morphology (Figure 1F, G). Instead, an agglomerated unidentified structure was observed (Figure 1G). This control experiment clearly indicates that PVPPh takes an important role during the formation of spherical NPs and then directs NPs to assemble into such chain-like structures.

We propose a possible mechanism for the formation of such long chain-like alloy nanostructures as given in Scheme 1. PVPPh is a solvent adoptable polymer with a phenol group on each alternative carbon atom of the chain. It is soluble in both aqueous and organic phase. The initial reaction system contains PVPPh,  $\text{Co}(\text{acac})_2$ , and  $\text{Ni}(\text{acac})_2$  dissolved in DMSO. As soon as aqueous hydrazine hydrate is added to the reaction mixture, the reduction of  $\text{Ni}(\text{acac})_2$  and  $\text{Co}(\text{acac})_2$  by hydrazine is taken place and forms small metal/alloy nuclei which eventually grow to form the NPs. The initially formed NiCo NPs are then interacted with the phenoxide ( $\text{PhO}^-$ ) groups of PVPPh (formed with the reaction of added NaOH) as shown in Scheme 1. This resulted in the adsorption of PVPPh molecules onto the surface of alloy NPs. Again, the PVPPh molecules are soluble in the reaction medium. Thus, the adsorbed PVPPh molecules help to prevent the aggregation of the formed alloy NPs through the steric interactions between the PVPPh molecules adsorbed onto the adjacent NPs. This results in the formation alloy NPs of

Scheme 1. Possible Mechanism for the Formation of Long Chainlike NiCo Alloy Nanostructures Using PVPh in DMSO/H<sub>2</sub>O

smaller size with good dispersity. However, our earlier method is an emulsion method, which usually produced particles of higher diameter and polydisperse in size.<sup>25</sup> Because the formed NPs (Ni or NiCo) are magnetic in nature, they assembled themselves to form chainlike structures through dipole–dipole interactions. From the MPMS measurement (see magnetic discussion portion later), it is found that the alloy NPs are soft ferromagnetic in nature and relatively more easy to polarize as the alloy NPs have low coercivity value (as mentioned later in this section). Also, the coercivity value of these alloy NPs are lower than that of alloys prepared with PVME as reported in our earlier paper.<sup>25</sup> Thus, in the present case, these NPs are very susceptible to orient their dipoles according to other magnetic dipoles and consequently long chainlike alloy nanostructures are formed.

The selected area electron diffraction (SAED) patterns, recorded from the specified portion (highlighted in red), showed the formation of nice bright rings (bottom inset of Figures 1A–G). The presence of such ringlike diffraction spots revealed the formation of polycrystalline face-centered cubic (fcc) Ni or NiCo alloy nanostructures.

EDS spectra (Figure S5 in the Supporting Information) of all the alloy samples (Table 1) show the presence of intense peaks due to elemental Co and Ni. There are also a Cu signals due to the use of Cu grid. The weight ratios of Ni to Co metals in samples PVPh-Ni<sub>3</sub>Co<sub>1</sub>, PVPh-Ni<sub>2</sub>Co<sub>1</sub>, PVPh-Ni<sub>1</sub>Co<sub>1</sub>, and PVPh-Ni<sub>1</sub>Co<sub>2</sub> are found to be 77: 23, 68: 32, 49:51, and 31: 69 respectively (Table 1). The calculated atomic ratios of Ni/Co in these samples are approximately equal to 3:1, 2:1, 1:1, and 1:2 respectively, which agrees well with target atomic ratios of Ni/Co as also observed for data obtained from ICP-OES measurements mentioned above (Table 1). For the control samples (Ni<sub>3</sub>Co<sub>1</sub> and Ni<sub>1</sub>Co<sub>1</sub>), the measured weight ratios of Ni/Co are 76:24 and 51:49, which also matches well with the target atomic ratios for the respective samples (Figure S5 in the Supporting Information).

The XRD patterns (Figure 2) of Ni/NiCo alloy samples show peaks at  $2\theta = 44.5, 51.9,$  and  $76.5^\circ$ , which can be indexed to (111), (200), and (220) planes of fcc metallic Ni as well as fcc metallic Co (JCPDS card nos. for fcc Ni and fcc Co are 04–

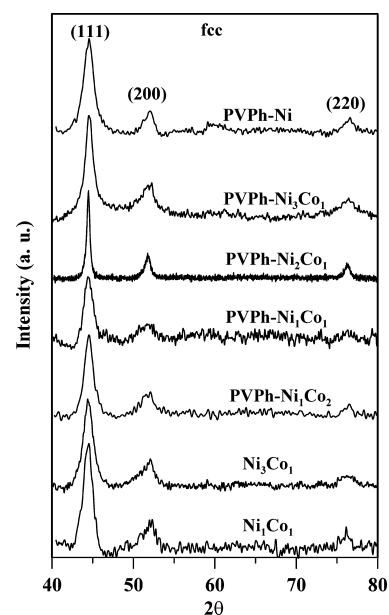
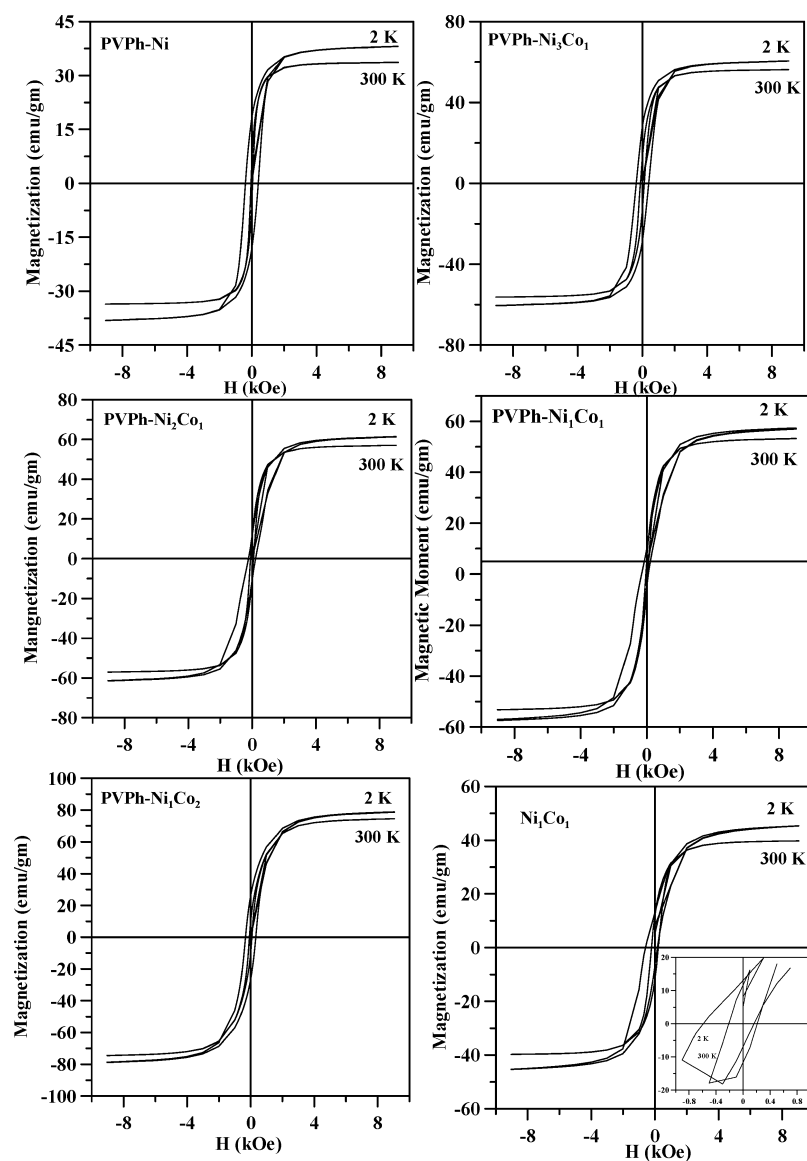


Figure 2. XRD patterns of Ni and NiCo alloy samples.

0850 and 15–0806). No other impurity peaks corresponding to hydroxides or oxides are observed. These peaks match well with the peaks of same alloys reported earlier.<sup>21,57</sup> The obtained alloys are fcc crystalline in nature since the lattice mismatch between monometallic Ni and Co is very small as also discussed by Zhang et al.<sup>20,21</sup> We also calculated the crystal grain sizes of these alloy samples from these XRD patterns using Scherrer's equation and the values are given in Table S1 in the Supporting Information. Table S1 in the Supporting Information reveals that the crystallite sizes of all the alloy samples are in the range of 6–7 nm, except a value of  $\sim 16$  nm is obtained for the PVPh-Ni<sub>2</sub>Co<sub>1</sub> sample.

We also investigate the magnetic properties of the neat Ni and NiCo alloy nanochains via magnetic property measurement system (MPMS). The magnetic responses of these materials were evaluated using an external magnetic field between  $\pm 10.0$  kOe. The saturation magnetization ( $M_s$ ) of all the



**Figure 3.** Magnetization hysteresis curves of different polymer magnetic Ni/NiCo alloy nanostructure (Table 2) at 2 and 300 K.

samples was measured at 2 and 300 K by cycling the field between  $\pm 10.0$  kOe. The isothermal magnetization data for the samples at 2K and 300 K are depicted in Figure 3. Table 2

**Table 2. Magnetization Properties of Monometallic Ni and Bimetallic NiCo Alloy Samples**

sample name	$M_s$ at 2 K ( $\text{emu g}^{-1}$ )	coercivity $H_c$ (Oe) at 2 K	$M_s$ at 300 K ( $\text{emu g}^{-1}$ )	coercivity $H_c$ (Oe) at 300 K
PVPh-Ni	38	791	34	103
PVPh-Ni <sub>3</sub> Co <sub>1</sub>	60	778	56	236
PVPh-Ni <sub>2</sub> Co <sub>1</sub>	61	433	57	173
PVPh-Ni <sub>1</sub> Co <sub>1</sub>	57	433	53	102
PVPh-Ni <sub>1</sub> Co <sub>2</sub>	79	637	74	153
Ni <sub>1</sub> Co <sub>1</sub>	45	743	40	445

summarizes the principal magnetic properties of these samples prepared both in presence and in absence of PVPh. It is clear that monometallic Ni and bimetallic NiCo alloy samples are ferromagnetic in nature (Figure 3). The saturation magnetization value for the PVPh-Ni sample is found to be

38 and 34  $\text{emu g}^{-1}$  at the temperatures 2 and 300 K (see Table 2). This saturation magnetization value (38  $\text{emu g}^{-1}$ ) is low compared to the bulk saturation magnetization of neat fcc Ni (63  $\text{emu g}^{-1}$ )<sup>25,58</sup> as also observed by other researcher.<sup>25,58</sup> This is probably due to the presence of nonmagnetic PVPh layer on monometallic Ni NPs. But with the increase of cobalt content in the alloys, the saturation bulk magnetization increases (Table 2). The saturation magnetization of Ni<sub>1</sub>Co<sub>1</sub> (45  $\text{emu g}^{-1}$ ) prepared without PVPh is much lower than that (57  $\text{emu g}^{-1}$ ) of PVPh-Ni<sub>1</sub>Co<sub>1</sub> at 2 K, although their compositions are nearly equal. This is probably because of the presence of an oxide layer at the surface of the Ni<sub>1</sub>Co<sub>1</sub> sample with unidentified structures compared to the well-defined chain-like PVPh-Ni<sub>1</sub>Co<sub>1</sub> alloy. The obtained neat Ni and NiCo alloy NPs show coercivity both in 2 and 300 K (Table 2). In every case the coercivity value in 2 K is higher than that obtained in 300 K. For PVPh-Ni samples, the coercivity value at 2 K is 791 Oe, which is very high compared to the values reported for the fcc Ni NPs by other researchers.<sup>17,20,31</sup> All other alloy samples show less coercivity compared to that of the monometallic Ni NPs.

Interestingly, the coercivity value is lowest for PVPh-Ni<sub>1</sub>Co<sub>1</sub> sample.

**Polymer Ni/NiCo Alloy Nanochain-Catalyzed Organic Reactions. Borohydride Reduction of *p*-Nitrophenol (4NP) in Water.** To study the catalytic activities of NiCo nanochain in water, we chose borohydride reduction of *p*-nitrophenol as a model reaction. This reaction has been extensively used by many research groups including us for studying activities of various metal NP catalysts.<sup>25,40,42,44–46,48</sup> In fact, we are the first to be able to report the rate constants of this reaction using NiCo alloys.<sup>25</sup> Time-dependent absorption spectra of this reaction (conducted at 25 °C) with different alloy or neat Ni samples show the decrease of absorbance of the peak at 400 nm, corresponding to *p*-nitrophenolate ion with time.<sup>40</sup> The time-dependent spectra of the *p*-nitrophenolate ion using different catalysts were given in Figure S6 of the Supporting Information. In the absence of this catalyst, this absorption band remains unaltered with time. We noticed an induction period of this reaction for each sample as depicted in Table 3.

**Table 3. Catalytic Rate Constants of the Borohydride Reduction of *p*-Nitrophenol in the Presence of Different Ni/NiCo Alloy Nanochain Samples**

sample name	amount (mg)	induction time (s)	$k_{app}^a$ (s <sup>-1</sup> )	$k_{nor}^b$ (mmol <sup>-1</sup> s <sup>-1</sup> )
PVPh-Ni	1.28	200	$3.45 \times 10^{-3}$	$2.03 \times 10^{-1}$
PVPh-Ni <sub>3</sub> Co <sub>1</sub>	1.3	10	$24.1 \times 10^{-3}$	$14.3 \times 10^{-1}$
PVPh-Ni <sub>2</sub> Co <sub>1</sub>	1.22	200	$5.03 \times 10^{-3}$	$2.96 \times 10^{-1}$
PVPh-Ni <sub>1</sub> Co <sub>1</sub>	0.97	80	$12.8 \times 10^{-3}$	$7.55 \times 10^{-1}$
PVPh-Ni <sub>1</sub> Co <sub>2</sub>	1.15	50	$15.7 \times 10^{-3}$	$9.26 \times 10^{-1}$
Ni <sub>3</sub> Co <sub>1</sub>	1.06	30	$9.17 \times 10^{-3}$	$5.41 \times 10^{-1}$
Ni <sub>1</sub> Co <sub>1</sub>	0.90	400	$1.8 \times 10^{-3}$	$1.18 \times 10^{-1}$

<sup>a</sup>Apparent rate constant. <sup>b</sup>Normalized rate constant.

Many research groups, including us have also noticed delay in start of this reaction in presence of catalyst.<sup>25,59,60</sup> The apparent rate constants of this reaction in presence of these catalysts were obtained from linear curves of  $\ln A_{400}$  versus time (Figure 4). We neglect the induction time during the construction of these plots (Figure 4). The values of apparent rate constants ( $k_{app}$ ) for the different samples are given in Table 3. For comparison, we normalized the apparent rate constants ( $k_{nor}$ ) with respect to the amount (mmol) of catalyst used. The  $k_{nor}$  values of different samples are also given in Table 3. It should be noted that the  $k_{nor}$  value for the sample PVPh-Ni<sub>3</sub>Co<sub>1</sub> is very high compared to that of other samples. This value is one of the highest so far reported for catalytic reduction of *p*-nitrophenol/borohydride system.<sup>25,40,43,44,46,61</sup> Note that the samples PVPh-Ni<sub>1</sub>Co<sub>1</sub> and PVPh-Ni<sub>1</sub>Co<sub>2</sub> show more or less similar catalytic activities (Table 3), except the sample PVPh-Ni<sub>3</sub>Co<sub>1</sub>, which shows slightly higher activity compared to the others. This higher activity of PVPh-Ni<sub>3</sub>Co<sub>1</sub> sample may be attributed to the smaller size of the alloy NPs that constituted the alloy nanochain. On the other hand, the sample (PVPh-Ni<sub>2</sub>Co<sub>1</sub>) exhibit comparatively less catalytic activity compared to the other alloy NPs samples. The probable reason is that this alloy NPs contains bigger crystallites (~16 nm) compared to other NiCo alloy NPs as calculated from the XRD measurement using Scherrer's equation (see Table S1 in the Supporting Information). However, these alloy samples also show higher activity compared to that of pure Ni sample although pure Ni NPs are smaller in size. This is probably the manifestation of

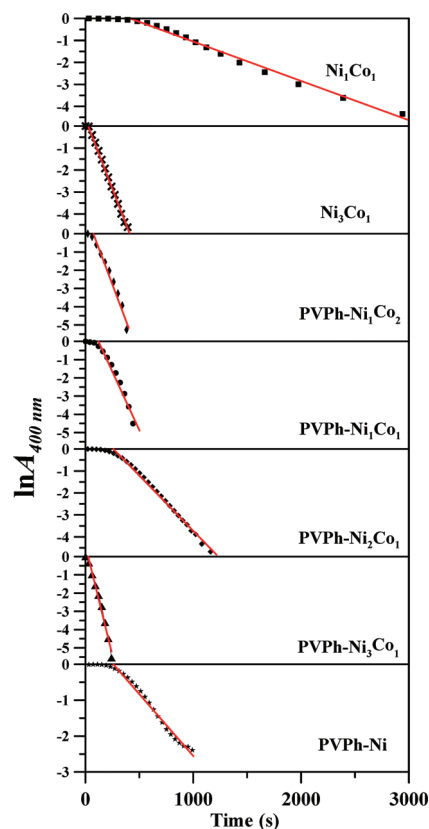


**Figure 4.** Plot showing the variation in  $\ln A$  with time for the borohydride reduction of 4NP catalyzed using Ni and different NiCo alloy nanochains. The absorbance of 4NP<sup>-</sup> ion was monitored at  $\lambda_{max} = 400$  nm.

the synergistic effects of alloy nanostructures, which shows higher activity compared to pure Ni samples. There is no noticeable effect of the presence of PVPh on the catalytic activities of the obtained alloy samples as the order of magnitude of the reaction rates of the borohydride reduction of *p*-nitrophenol using alloy catalysts, prepared with and without PVPh are almost similar (see Table 3). The reason is that the thickness of the PVPh layer on the surface of alloy NPs is very small. Thus, we can assume that the higher activity of the alloy nanochains prepared with PVPh is the manifestation of the controlled size effect of these alloy NPs (see Table 3).

To calculate the activation energy the nanocatalyst (PVPh-Ni<sub>3</sub>Co<sub>1</sub>), we performed the reactions at four different temperatures, such as 25, 35, 45, and 55 °C. The successive decrease of the absorbance at 400 nm with time has been plotted in Figure S7 in the Supporting Information. The  $k_{nor}$  values for this reaction at these temperatures were obtained by similarly as above (Figure 5A). The calculated  $k_{nor}$  values at different temperatures were then plotted as  $\ln k_{nor}$  against  $1000/T$  (Figure 5B). The activation energy of the reaction for the catalyst PVPh-Ni<sub>3</sub>Co<sub>1</sub> was calculated (from the slope) to be 31.9 kJ/mol. This value is also low compared to that reported for this *p*-nitrophenol reduction reaction when Pt, Pd, Au, and Ag NPs catalyst were used.<sup>44,45,60</sup> But for gold nanocages, the activation energy value (28 kJ/mol) is slightly lower than our obtained value (31.9 kJ/mol).<sup>60</sup> The entropy of activation of this *p*-nitrophenol reduction reaction using the catalyst PVPh-Ni<sub>3</sub>Co<sub>1</sub> was calculated to be 67.2 J/mol K, which is also lower compared to the values reported by others.<sup>44,60</sup>

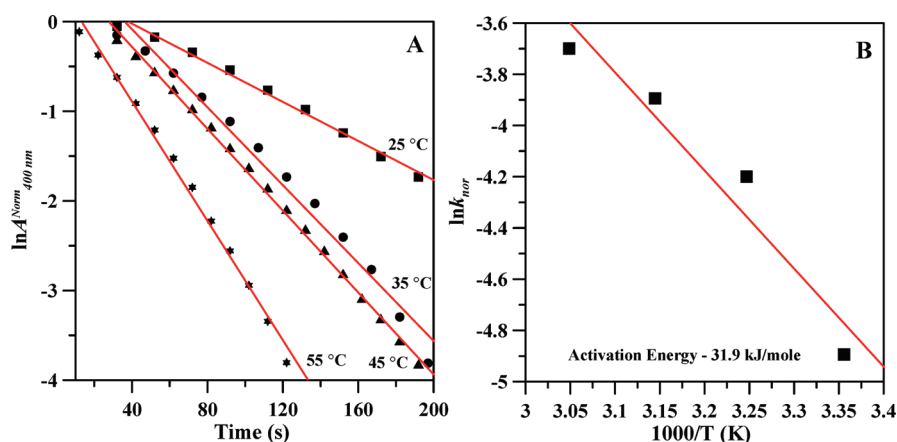


**Figure 5.** (A) Plots of  $\ln A$  ( $A$  = absorbance at 400 nm of *p*-nitrophenolate ion) versus time for the reduction of *p*-nitrophenol using PVPh-Ni<sub>3</sub>Co<sub>1</sub> nanocatalyst at four different temperatures. (B) Plot showing the variation of  $\ln k_{\text{nor}}$  with  $1000/T$  for this reduction reaction constructed from the plots in panel A.

**C–S Cross-Coupling Reactions of Aryl Thiols with Aryl Iodides in Organic Medium.** In our preliminary study, we found that the S-aryl cross-coupling reaction of phenyl iodide with *p*-chlorothiophenol using short NiCo alloy nanochain occurred to afford the cross-coupled product in very low yield (30%).<sup>25</sup> This result prompted us to further study to increase the yield of this reaction as well as to study in detail the scope of NiCo alloy NPs for the catalysis of the C–S cross-coupling reaction using different substituted aryl iodides and thiophenols. For this, we used the as-synthesized long NiCo alloy nanochains constituted of more monodisperse spherical alloy NPs of smaller size compared to that we reported previously.<sup>25</sup> To improve the yield, we first optimized the reaction conditions. Using a representative catalyst PVPh-Ni<sub>3</sub>Co<sub>1</sub>, we conducted the reaction of phenyl iodide with *p*-chlorothiophenol in three different organic media such as pure DMF, (1:1) mixture of DMF and acetonitrile and (1:3) mixture of DMF and dioxin. The yields of *s*-arylated product (4-chlorodiphenyl sulfide) in these solvents after 15 h were 60, 91, and 25%, respectively. Note that the yields of this reaction using PVPh-Ni<sub>3</sub>Co<sub>1</sub> in DMF and acetonitrile (1:1) mixture after 3 and 8 h were only 25 and 64% respectively. Thus, we used a reaction time of 15 h and a (1:1) mixture of DMF/acetonitrile as solvent. The NMR spectrum and analysis data of 4-chlorodiphenyl sulfide are given in page S11 of the Supporting Information. Similarly, PVPh-Ni and other PVPh-NiCo alloy samples were also used to investigate this cross-coupling reaction and the obtained yields are given in Table 4. The reactions preceded smoothly yielding *s*-arylated product with up to 96% yield when PVPh-Ni<sub>1</sub>Co<sub>2</sub> alloy nanochain was used as catalyst. Also, the yields are almost independent of composition of Ni and Co in the alloy used for catalysis. When the reaction was performed with Ni<sub>3</sub>Co<sub>1</sub> and Ni<sub>1</sub>Co<sub>1</sub> control samples, the measured yield of *s*-arylated product were only 75 and 55%. These results confirm the effects of the polymer on the structure of the synthesized alloy nanochains and the effect of the irregular morphology on the catalytic activities of Ni<sub>3</sub>Co<sub>1</sub> and Ni<sub>1</sub>Co<sub>1</sub> toward the C–S cross-coupling reactions.

Finally, the C–S cross-coupling reactions of different thiophenols and aryl iodides were studied using a representative sample PVPh-Ni<sub>3</sub>Co<sub>1</sub>. In most of the cases, we get good to excellent yields of the C–S cross-coupled product (Table 5). All the products are characterized via NMR spectroscopy

**Table 4.** Cross-Coupling Reaction of Phenyl Iodide with *p*-Chlorothiophenol Using Different Ni/NiCo Alloy Nanochain Samples

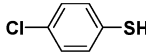
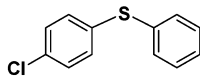
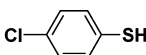
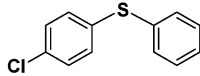
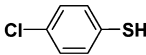
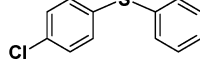
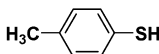
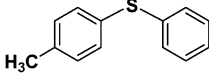
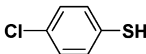
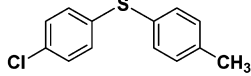
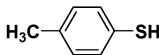
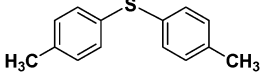
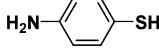
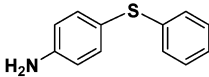
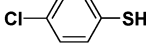
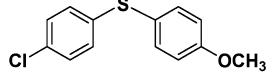
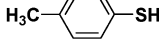
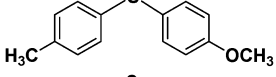
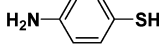
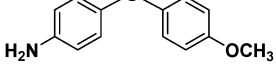
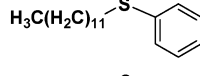
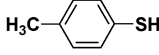
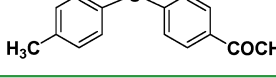
sample name	yield of 4-chlorodiphenyl sulfide (%)
PVPh-Ni	87
PVPh-Ni <sub>3</sub> Co <sub>1</sub>	91
PVPh-Ni <sub>2</sub> Co <sub>1</sub>	85
PVPh-Ni <sub>1</sub> Co <sub>1</sub>	92
PVPh-Ni <sub>1</sub> Co <sub>2</sub>	96
Ni <sub>3</sub> Co <sub>1</sub>	75
Ni <sub>1</sub> Co <sub>1</sub>	55

(Pages S11–S23 in the Supporting Information). When the substituted aryl thiols contain chloro and methyl groups, the yields of the products were good (except entry 3) as the resultant thiolate ions were stabilized as shown in Scheme 2. A careful examination for the entry no. 2, 4, and 7 in Table 5 showed that the –H, –CH<sub>3</sub> and –OCH<sub>3</sub> substitution at the para-position of the aryl iodide gives a good to better yield of the products diaryl sulfides. When an electron withdrawing group (–COCH<sub>3</sub>) is present in the para-position, we did not get any desired product (entry 10). This is may be due to the fact that the oxidative addition of the aryl iodide decreases due to the presence of acetyl group (see mechanism section). Thus, for the electron donating groups in aryl iodides, such as, CH<sub>3</sub> and OCH<sub>3</sub>, we observed good yield of the products. Our catalyst is also useful for the cross-coupling reactions with long-chain alkyl thiols (dodecane thiol), but the yield is about 30% (Table 5, entry 9).

**C–O Cross-Coupling Reaction of 3,5-Dimethyl-phenol with Iodobenzene in Organic Medium.** To check whether the obtained NiCo nanochain catalyst can be equally effective for the C–O cross-coupling reactions, we carried out the following experiment. The C–O cross-coupling reaction of 3,5-dimethylphenol with iodobenzene was investigated using PVPh-Ni<sub>3</sub>Co<sub>1</sub> as a representative case (Scheme 3). The reaction occurred smoothly with the formation of O-arylated product (1,3-dimethyl-5-phenoxy-benzene), but yield is very poor (~20%).



Table 5. C–S Cross-Coupling Reactions of Substituted Aryl Thiols with Substituted Aryl Iodides Using PVPh-Ni<sub>3</sub>Co<sub>1</sub> Alloy Sample

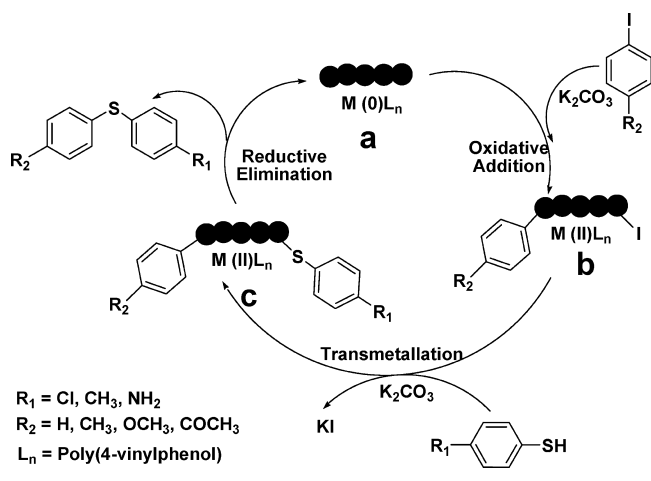
$\text{R}_1\text{-SH} + \text{I}-\text{C}_6\text{H}_4\text{-R}_2 \xrightarrow[\text{DMF : CH}_3\text{CN} = 1:1, 110^\circ\text{C}]{\text{K}_2\text{CO}_3, \text{PVPh-Ni}_3\text{Co}_1}$				$\text{R}_1\text{-C}_6\text{H}_4\text{-S-C}_6\text{H}_4\text{-R}_2$	
Entry	R <sub>1</sub> -SH	R <sub>2</sub>	Time (h)	Product	Yields (%)
1		H	3		25
		H	8		64
		H	15		91
2		H	15		98
3		CH <sub>3</sub>	15		36
4		CH <sub>3</sub>	15		95
5		H	15		70
6		OCH <sub>3</sub>	15		92
7		OCH <sub>3</sub>	15		73
8		OCH <sub>3</sub>	15		76
9	$\text{H}_3\text{C(H}_2\text{C)}_{11}\text{-SH}$	H	15		30
10		COCH <sub>3</sub>	15		-

A control experiment using Ni<sub>3</sub>Co<sub>1</sub> alloy (without polymer) was performed using similar reaction condition for the O-arylation reaction. But, the yield is only about 4%. These results reveal that the synthesized NiCo alloy nanochains can also catalyze the C–O cross-coupling reaction in organic solvent. Presently, we are trying to improve the yield of this reaction by varying the temperature and reaction medium. The detail investigation of this NiCo catalyzed C–O cross-coupling reaction using different substrates is also underway.

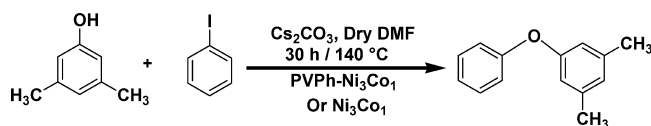
**Mechanism.** While considering the mechanism of this bimetallic alloy catalyzed cross-coupling reactions, we encountered two types of mechanism (although similar) that have been proposed by other researcher.<sup>62,63</sup> Bhadra et al. proposed a mechanism in which organic thiophenol is coordinated with the metal NPs first.<sup>63</sup> Organic halide then also gets coordinated with the metal NPs. Finally, the product is formed via reductive elimination pathway.<sup>63</sup> In another proposed pathway, the oxidative addition of organic halide to metal NPs occurs first

and consequently, the metal gets oxidized to its higher oxidation states. Organic thiophenol then gets coordinated to the oxidized metal surface through transmetalation.<sup>62</sup> The cross-coupled product is formed through the reductive elimination and metal gets reduced to its zerovalent state.<sup>62</sup> Because of the presence of some contradiction in the two mechanisms, while proposing a mechanism for our case, we performed some control experiments. First, we measured the zeta potential of the catalyst PVPh-Ni<sub>3</sub>Co<sub>1</sub> by dispersing in DMF and acetonitrile (1:1) mixture. The obtained zeta potential value is +42 mV (see Figure S8 in the Supporting Information). The positive zeta potential indicates positive surface charges for the alloy nanostructures and may be caused by the adsorption of positive ions, such as, Ni<sup>2+</sup> or Co<sup>2+</sup>. The catalyst PVPh-Ni<sub>3</sub>Co<sub>1</sub> was then mixed with iodobenzene and K<sub>2</sub>CO<sub>3</sub> in the solvent mixture and was heated at 110 °C. The zeta potential of PVPh-Ni<sub>3</sub>Co<sub>1</sub> was then measured after cooling. Surprisingly, we got the value of –53 mV (Figure S8 in the

**Scheme 2. Possible Mechanism for NiCo Alloy Nanochain Catalyzed Cross-Coupling Reaction in (1:1) DMF and Acetonitrile Mixture at 110 °C**



**Scheme 3. Cross-Coupling Reaction between 3,5-Dimethylphenol and Iodobenzene in Dry DMF Using PVPh-Ni<sub>3</sub>Co<sub>1</sub> and Ni<sub>3</sub>Co<sub>1</sub> Alloy As a Catalyst**



Supporting Information). This indicates the adsorption of iodobenzene on to the surface of alloy NPs. We then separately heated the mixture of alloy sample with 4-chlorothiophenol and  $K_2CO_3$  at 110 °C. The measured zeta potential of the PVPh-Ni<sub>3</sub>Co<sub>1</sub> alloy after cooling is -26 mV. This indicates that thiophenol also get coordinated at the surface of the alloy NPs, But it is the iodobenzene which better coordinated with the alloy NPs under the same reaction conditions. From the results of these control experiments, we propose a tentative mechanism for the C-S bond formation using PVPh adsorbed NiCo alloy nanostructures as pseudo-heterogeneous/heterogeneous catalysts as shown in the Scheme 2. The mechanism is similar to that proposed by Beletskaya et al.<sup>62</sup> From the zeta potential measurements, it is clear that the surface of the NiCo alloy nanostructures is positively charged and the polymer PVPh is coordinated with the nanostructures. The solvent stabilized NiCo alloy nanochain  $[M(0)L_n]$  (a) undergo reaction with aryl iodide via oxidative addition in presence of base  $K_2CO_3$ . Consequently, the M(0) gets oxidized to form metal complex  $[Ar_1 M(II)I]$  (b). Then, in the presence of base  $K_2CO_3$ , transmetalation of arylthiol occurs into the metal complex b to form the metal complex  $[Ar_1 M(II)SAr_2]$  (c). Finally, carbon-sulfur reductive elimination of the thioether occurs from complex c to get back the metal alloys  $[M(0)L_n]$ .<sup>62,64</sup>

**Reusability Study.** The obtained NiCo alloy catalysts are reusable. A representative sample PVPh-Ni<sub>3</sub>Co<sub>1</sub> is used to test for reusability in the borohydride reduction of 4-NP and the alloy NPs was recovered using a bar magnet. The recovered, washed, and dried alloy NPs was then reused to carry out the fresh borohydride reduction of 4-NP another six times. After completion of all seven cycles, we found that only about 6% loss in weight of the initial alloy used. The apparent rate constant of the reaction in each cycle was measured by similar method as mentioned above. Considering about 1 wt % loss in

each cycle, the normalized rate constants in each cycle were measured and were plotted against the number of cycle (Figure 6).

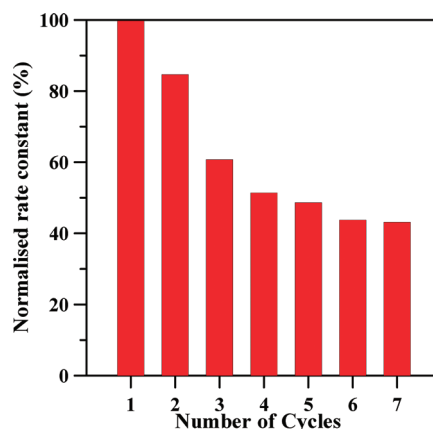


**Figure 6.** Plot showing the variation in normalized rate constant in different cycles of the borohydride reduction of *p*-nitrophenol using PVPh-Ni<sub>3</sub>Co<sub>1</sub> sample.

It is clear that after seven cycles of reuse, the alloy NPs show around 45% activity of its virgin activity. The NiCo catalyst still remains active for the reaction, although the activity decreases to some extent. One of the reviewer questioned whether the decrease of activity of catalyst is due to the damage of the chain structures and particles after reaction cycles. To check this we examined the alloy NPs after catalysis using TEM (see Figure S9A in the Supporting Information). We hardly found any difference in the particle size and the chain structure to that of the sample PVPh-Ni<sub>3</sub>Co<sub>1</sub> before and after catalysis (compare Figure 1A with Figure S9A in the Supporting Information). Thus, it is difficult to say that the stability of the structure of the alloy catalysts decreases after reaction rather some other factor is responsible for this decrease in activity. Further, we try to clarify this issue by performing some control experiments. We performed the reduction of *p*-nitrophenol using the alloy catalyst in N<sub>2</sub> atmosphere and also reused the same catalyst by performing the reaction again in N<sub>2</sub> atmosphere. We found that the decrease of the reaction rate is very small even after fifth cycle of reuse (see Figure S10 in the Supporting Information). This is probably due to the fact that in N<sub>2</sub> atmosphere, the rate of surface oxidation of the alloy is less and thus it maintains nearly similar catalytic activities. Thus, we can conclude that it is the aerial oxygen which make the catalyst's surface inactive during the course of the reaction and form an oxide layer around the catalysts. This is the reason why the EDS analysis data (Figure S9B in the Supporting Information) shows the higher amount of oxygen (4 wt %) present in the catalyst after the reusability test.

## CONCLUSIONS

Solvent-adoptable long nanochains consisting of bimetallic NiCo alloy nanoparticles were synthesized by a simple one-pot solution phase reduction method in the presence of polymer. Monometallic Ni nanochain was also prepared by similar method. Elemental compositions of nanoalloys can be easily tuned by changing the initial molar ratios of Ni to Co precursors and was determined via ICP-OES and EDS measurements. The formation of long chainlike Ni/NiCo alloy nanostructures composed of respective nanoparticles was confirmed via TEM and FESEM. NiCo alloy samples prepared without

the polymer, PVPh, did not show chainlike morphology. The obtained Ni or NiCo alloy samples were polycrystalline in nature. The magnetic measurements revealed ferromagnetic nature of the obtained Ni and NiCo alloy nanostructures. Because of adsorbed PVPh, the obtained Ni and NiCo alloy nanostructures can be easily redispersed in both water and organic solvents. This makes them more versatile to be used as catalysts in both aqueous and nonaqueous media. The Ni and NiCo alloy nanochains showed very high catalytic activity in the borohydride reduction of *p*-nitrophenol in water. The C–S cross-coupling reactions of various aryl thiols with aryl iodides in organic media occurred very smoothly in presence of as-synthesized Ni or NiCo alloy nanochain catalysts to afford the corresponding cross-coupled products in good to excellent yield. We are the first to report this type of Ni/NiCo alloy catalyzed C–S cross-coupling reaction with very high yield. Our catalyst also successfully catalyzed the C–O cross-coupling reaction in organic medium. The NiCo alloy catalyst is magnetically recoverable and reusable.

## ■ ASSOCIATED CONTENT

### ■ Supporting Information

The size of the crystallites for different alloy samples calculated from XRD patterns, photographs of dispersions of the sample PVPh-Ni<sub>3</sub>Co<sub>1</sub> in different solvents, FTIR spectra of PVPh-Ni<sub>1</sub>Co<sub>1</sub> and neat PVPh, low-magnification TEM and SEM images of different alloy NPs to show long-chain formation, histograms of particle size distribution of spherical NPs of nanochains, formation mechanism of the long-chain alloy NPs, EDS spectra of Ni/NiCo alloy nanochains, successive UV–vis spectra for borohydride reduction of *p*-nitrophenol in the presence of Ni/NiCo alloy samples, zeta potential of the sample PVPh-Ni<sub>3</sub>Co<sub>1</sub>, TEM image and EDS analysis of the sample PVPh-Ni<sub>3</sub>Co<sub>1</sub> after catalysis, reusability study of the sample PVPh-Ni<sub>3</sub>Co<sub>1</sub> under N<sub>2</sub> atmosphere, <sup>1</sup>H NMR and <sup>13</sup>C NMR spectra of all diaryl sulfides and their analysis data. This material is available free of charge via the Internet at <http://pubs.acs.org>.

## ■ AUTHOR INFORMATION

### Corresponding Author

\*E-mail: [psutkm@iacs.res.in](mailto:psutkm@iacs.res.in). Fax: (+91) 33-2473-2805.

## ■ ACKNOWLEDGMENTS

M.R., S.L., and M.R. acknowledge CSIR, Government of India, for providing Research Fellowships. This research was supported by the grant from the DST, New Delhi, India, under the Nanoscience and Nanotechnology Initiative. We also thank the reviewer who offered constructive criticism and suggested additional experiments, which were duly performed as described in the text.

## ■ REFERENCES

- (1) Cortie, M. B.; McDonagh, A. M. *Chem. Rev.* **2011**, *111*, 3713.
- (2) Comstock, R. L. *J. Mater. Sci.: Mater. Electron* **2002**, *13*, 509.
- (3) Weller, D.; Moser, A. *IEEE Trans. Magn.* **1999**, *35*, 4423.
- (4) Fang, C.; Zhang, M. *J. Mater. Chem.* **2009**, *19*, 6258.
- (5) Ito, A.; Shinkai, M.; Honda, H.; Kobayashi, T. *J. Biosci. Bioeng.* **2005**, *100*, 1.
- (6) Roucoux, A.; Schulz, J.; Patin, H. *Chem. Rev.* **2002**, *102*, 3757.
- (7) Heemeier, M.; Carlsson, A. F.; Naschitzki, M.; Schmal, M.; Bäumer, M.; Freund, H.-J. *Angew. Chem., Int. Ed.* **2002**, *41*, 4073.
- (8) Hong, R.; Fischer, N. O.; Emrick, T.; Rotello, V. M. *Chem. Mater.* **2005**, *17*, 4617.
- (9) Ferrando, R.; Jellinek, J.; Johnston, R. L. *Chem. Rev.* **2008**, *108*, 845.
- (10) Yan, J.-M.; Zhang, X.-B.; Akita, T.; Haruta, M.; Xu, Q. *J. Am. Chem. Soc.* **2010**, *132*, 5326.
- (11) Su, X. B.; Zheng, H. G.; Yang, Z. P.; Zhu, Y. C.; Pan, A. L. *J. Mater. Sci.* **2003**, *38*, 4581.
- (12) Cheng, F.; Ma, H.; Li, Y.; Chen, J. *Inorg. Chem.* **2007**, *46*, 788.
- (13) Lu, P.; Teranishi, T.; Asakura, K.; Miyake, M.; Toshima, N. *J. Phys. Chem. B* **1999**, *103*, 9673.
- (14) Ennas, G.; Falqui, A.; Paschina, G.; Marongiu, G. *Chem. Mater.* **2005**, *17*, 6486.
- (15) Shevchenko, E. V.; Talapin, D. V.; Rogach, A. L.; Kornowski, A.; Haase, M.; Weller, H. *J. Am. Chem. Soc.* **2002**, *124*, 11480.
- (16) Hu, M. J.; Lin, B.; Yu, S. H. *Nano Res.* **2008**, *1*, 303.
- (17) Mattei, G.; de Julian Fernandez, C.; Mazzoldi, P.; Sada, C.; De, G.; Battaglin, G.; Sangregorio, C.; Gatteschi, D. *Chem. Mater.* **2002**, *14*, 3440.
- (18) Syukri, Ban, T.; Ohya, Y.; Takahashi, Y. *Mater. Chem. Phys.* **2003**, *78*, 645.
- (19) Wei, X.-W.; Zhou, X.-M.; Wu, K.-L.; Chen, Y. *CrystEngComm* **2011**, *13*, 1328.
- (20) Yamauchi, T.; Tsukahara, Y.; Yamada, K.; Sakata, T.; Wada, Y. *Chem. Mater.* **2011**, *23*, 75.
- (21) Zhang, H.; Yao, T.; Sun, Z.; Li, Y.; Liu, Q.; Hu, F.; Pan, Z.; He, B.; Xie, Z.; Wei, S. *J. Phys. Chem. C* **2010**, *114*, 13596.
- (22) Zhu, L.-P.; Xiao, H.-M.; Fu, S.-Y. *Eur. J. Inorg. Chem.* **2007**, *2007*, 3947.
- (23) Carroll, K. J.; Calvin, S.; Ekiert, T. F.; Unruh, K. M.; Carpenter, E. E. *Chem. Mater.* **2010**, *22*, 2175.
- (24) Bagkar, N.; Seo, K.; Yoon, H.; In, J.; Jo, Y.; Kim, B. *Chem. Mater.* **2010**, *22*, 1831.
- (25) Rashid, M. H.; Raula, M.; Mandal, T. K. *J. Mater. Chem.* **2011**, *21*, 4904.
- (26) Ahmed, J.; Sharma, S.; Ramanujachary, K. V.; Lofland, S. E.; Ganguli, A. K. *J. Colloid Interface Sci.* **2009**, *336*, 814.
- (27) Viau, G.; Fiévet-Vincent, F.; Fiévet, F. *Solid State Ionics* **1996**, *84*, 259.
- (28) Hu, M.-J.; Lu, Y.; Zhang, S.; Guo, S.-R.; Lin, B.; Zhang, M.; Yu, S.-H. *J. Am. Chem. Soc.* **2008**, *130*, 11606.
- (29) Sharma, S.; Gajbhiye, N. S.; Ningthoujam, R. S. *J. Colloid Interface Sci.* **2010**, *351*, 323.
- (30) Samia, A. C. S.; Schlueter, J. A.; Jiang, J. S.; Bader, S. D.; Qin, C.-J.; Lin, X.-M. *Chem. Mater.* **2006**, *18*, 5203.
- (31) Brayner, R.; Vaulay, M.-J.; Fievet, F.; Coradin, T. *Chem. Mater.* **2007**, *19*, 1190.
- (32) Sarkar, A.; Kapoor, S.; Yashwant, G.; Salunke, H. G.; Mukherjee, T. *J. Phys. Chem. B* **2005**, *109*, 7203.
- (33) Murray, C. B.; Sun, S. H.; Doyle, H.; Betley, T. *MRS Bull.* **2001**, *26*, 985.
- (34) Wei, X.-W.; Zhu, G.-X.; Liu, Y.-J.; Ni, Y.-H.; Song, Y.; Xu, Z. *Chem. Mater.* **2008**, *20*, 6248.
- (35) Burke, N. A. D.; Stover, H. D. H.; Dawson, F. P. *Chem. Mater.* **2002**, *14*, 4752.
- (36) Bhattacharjee, R. R.; Chakraborty, M.; Mandal, T. K. *J. Nanosci. Nanotech.* **2004**, *4*, 844.
- (37) Kondo, T.; Mitsudo, T. A. *Chem. Rev.* **2000**, *100*, 3205.
- (38) Narayanan, R.; El-Sayed, M. A. *J. Phys. Chem. B* **2005**, *109*, 12663.
- (39) Ranu, B. C.; Saha, A.; Jana, R. *Adv. Synth. Catal.* **2007**, *349*, 2690.
- (40) Rashid, M. H.; Mandal, T. K. *Adv. Funct. Mater.* **2008**, *18*, 2261.
- (41) Zhou, P.; Li, Y.; Sun, P.; Zhou, J.; Bao, J. *Chem. Commun.* **2007**, 1418.
- (42) Esumi, K.; Isono, R.; Yoshimura, T. *Langmuir* **2004**, *20*, 237.
- (43) Jana, D.; Dandapat, A.; De, G. *Langmuir* **2010**, *26*, 12177.
- (44) Mahmoud, M. A.; Saira, F.; El-Sayed, M. A. *Nano Lett.* **2010**, *10*, 3764.
- (45) Rashid, M. H.; Mandal, T. K. *J. Phys. Chem. C* **2007**, *111*, 16750.

- (46) Sarkar, S.; Sinha, A. K.; Pradhan, M.; Basu, M.; Negishi, Y.; Pal, T. *J. Phys. Chem. C* **2011**, *115*, 1659.
- (47) Zhou, X.; Xu, W.; Liu, G.; Panda, D.; Chen, P. *J. Am. Chem. Soc.* **2010**, *132*, 138.
- (48) Wu, K.-L.; Wei, X.-W.; Zhou, X.-M.; Wu, D.-H.; Liu, X.-W.; Ye, Y.; Wang, Q. *J. Phys. Chem. C* **2011**, *115*, 16268.
- (49) Liu, G.; Link, J. T.; Pei, Z.; Reilly, E. B.; Leitza, S.; Nguyen, B.; Marsh, K. C.; Okasinski, G. F.; von Geldern, T. W.; Ormes, M.; Fowler, K.; Gallatin, M. *J. Med. Chem.* **2000**, *43*, 4025.
- (50) Bringmann, G.; Walter, R.; Weirich, R. *Angew. Chem., Int. Ed.* **1990**, *29*, 977.
- (51) Evano, G.; Blanchard, N.; Toumi, M. *Chem. Rev.* **2008**, *108*, 3054.
- (52) Wang, Y.; Chackalamannil, S.; Chang, W.; Greenlee, W.; Ruperto, V.; Duffy, R. A.; McQuade, R.; Lachowicz, J. E. *Bioorg. Med. Chem. Lett.* **2001**, *11*, 891.
- (53) Kidwai, M.; Mishra, N. K.; Bansal, V.; Kumar, A.; Mozumdar, S. *Tetrahedron Lett.* **2007**, *48*, 8883.
- (54) Takagi, K. *Chem. Lett.* **1987**, *16*, 2221.
- (55) Gestoso, P.; Brisson, J. *Polymer* **2001**, *42*, 8415.
- (56) Einhäuser, T. J. *Microchim. Acta* **1997**, *127*, 265.
- (57) Li, X. G.; Murai, T.; Chiba, A.; Takahashi, S. *J. Appl. Phys.* **1999**, *86*, 1867.
- (58) Cordente, N.; Respaud, M.; Senocq, F.; Casanove, M.-J.; Amiens, C.; Chaudret, B. *Nano Lett.* **2001**, *1*, 565.
- (59) Wunder, S.; Polzer, F.; Lu, Y.; Mei, Y.; Ballauff, M. *J. Phys. Chem. C* **2010**, *114*, 8814.
- (60) Zeng, J.; Zhang, Q.; Chen, J.; Xia, Y. *Nano Lett.* **2010**, *10*, 30.
- (61) Qin, G. W.; Pei, W.; Ma, X.; Xu, X.; Ren, Y.; Sun, W.; Zuo, L. *J. Phys. Chem. C* **2010**, *114*, 6909.
- (62) Beletskaya, I. P.; Ananikov, V. P. *Chem. Rev.* **2011**, *111*, 1596.
- (63) Bhadra, S.; Sreedhar, B.; Ranu, B. C. *Adv. Synth. Catal.* **2009**, *351*, 2369.
- (64) Wong, Y.-C.; Jayanth, T. T.; Cheng, C.-H. *Org. Lett.* **2006**, *8*, 5613.